Received: 20 July 2021 | Accepted: 24 January 2022

DOI: 10.1002/pros.24314

ORIGINAL ARTICLE

The Prostate WILEY

Development of a novel castration-resistant orthotopic prostate cancer model in New Zealand White rabbit

Yu Wang MD, PhD[1,2] | Eric C. Abenojar PhD[1] | Jing Wang BSc[1] | Al C. de Leon PhD[1] | Sidhartha Tavri MD[1] | Xinning Wang PhD[3] | Ramamurthy Gopalakrishnan PhD[1] | Ethan Walker PhD[3] | Gregory T. MacLennan MD[4] | Anoja Giles BSc[5] | Gregory J. Czarnota MD, PhD[5,6] | James P. Basilion PhD[1,3] | Agata A. Exner PhD[1,3]

[1]Department of Radiology, Case Western Reserve University, Cleveland, Ohio, USA

[2]Department of Ultrasound, Peking University People's Hospital, Beijing, China

[3]Department of Biomedical Engineering, Case Western Reserve University, Cleveland, Ohio, USA

[4]Department of Pathology and Urology, University Hospitals Cleveland Medical Center, Case Western Reserve University, Cleveland, Ohio, USA

[5]Physical Sciences, Sunnybrook Research Institute, Toronto, Ontario, Canada

[6]Departments of Radiation Oncology and Medical Biophysics, University of Toronto, Toronto, Ontario, Canada

Correspondence

Agata A. Exner, PhD, Department of Radiology, Case Western Reserve University, Cleveland, OH 44106, USA.
Email: agata.exner@case.edu

Funding information

National Institute of Biomedical Imaging and Bioengineering, Grant/Award Number: R01EB025741; Case-Coulter Translational Research Partnership

Abstract

Background: Prostate cancer (PCa) models in mice and rats are limited by their size and lack of a clearly delineated or easily accessible prostate gland. The canine PCa model is currently the only large animal model which can be used to test new preclinical interventions but is costly and availability is sparse. As an alternative, we developed an orthotopic human prostate tumor model in an immunosuppressed New Zealand White rabbit. Rabbits are phylogenetically closer to humans, their prostate gland is anatomically similar, and its size allows for clinically-relevant testing of interventions.

Methods: Rabbits were immunosuppressed via injection of cyclosporine. Human PC3pipGFP PCa cells were injected into the prostate via either (a) laparotomy or (b) transabdominal ultrasound (US) guided injection. Tumor growth was monitored using US and magnetic resonance imaging (MRI). Contrast-enhanced ultrasound (CEUS) imaging using nanobubbles and Lumason microbubbles was also performed to examine imaging features and determine the optimal contrast dose required for enhanced visualization of the tumor. Ex vivo fluorescence imaging, histopathology, and immunohistochemistry analyses of the collected tissues were performed to validate tumor morphology and prostate-specific membrane antigen (PSMA) expression.

Results: Immunosuppression and tumor growth were, in general, well-tolerated by the rabbits. Fourteen out of 20 rabbits, with an average age of 8 months, successfully grew detectable tumors from Day 14 onwards after cell injection. The tumor growth rate was $39 \pm 25\ mm^2$ per week. CEUS and MRI of tumors appear hypoechoic and T2 hypointense, respectively, relative to normal prostate tissue. Minimally invasive US-guided tumor cell injection proved to be a better method compared to laparotomy due to the shorter recovery time required for the rabbits following injection. Among the rabbits that grew tumors, seven had tumors both inside and outside the prostate, three had tumors only inside the prostate, and four had tumors exclusively outside of the prostate. All tumors expressed the PSMA receptor.

Yu Wang, Eric C. Abenojar, Jing Wang, and Al C. de Leon contributed equally to this study.

Conclusions: We have established, for the first time, an orthotopic PCa rabbit model via percutaneous US-guided tumor cell inoculation. This animal model is an attractive, clinically relevant intermediate step to assess preclinical diagnostic and therapeutic compounds.

KEYWORDS
contrast-enhanced ultrasound, magnetic resonance imaging, nanobubbles, orthotopic prostate cancer, rabbit model

1 | INTRODUCTION

Prostate cancer (PCa) exhibits the highest incidence rate of all cancers in American men, with over 3,200,000 men living with PCa today in the United States alone.[1] While significant improvements have been made in the management of PCa in the past decade, unmet needs remain for both diagnosis and therapy. For example, standard PCa biopsy procedures use ultrasound (US) guidance to determine prostate gland orientation, but the delineation of tumors within the prostate using the US is unclear.[2–4] As such, prostate biopsies remain mostly without specific delineation of target lesions and still result in significant false negatives upwards of 50%.[5] More precise localization of cancer within the current physician workflow would inform staging and biopsies, which represent a critical step in the subsequent treatment and outcomes of PCa. Moreover, despite relatively high 5-year survival rates, PCa is the second most common cause of cancer-related deaths among American males.[6] Androgen deprivation therapy has been proven highly effective as the first line of treatment for patients with advanced-stage PCa who are not eligible for radiation or prostatectomy. This treatment takes advantage of the fact that androgen signaling is essential for PCa growth and facilitates antiapoptotic mechanisms within the tumor.[7] However, despite significant initial responses, nearly all patients that receive this treatment later develop castration resistant cancer and androgen ablation therapy fails. This, in turn, leads to the recurrence and/or progression of castration-resistant PCa (CRPC).[8] CRPC, therefore, represents a stage in the continuum of the disease that is deadly. CRPC is defined by consecutive rises in serum prostate-specific antigen levels and/or progression of metastatic spread in the setting of castration levels of testosterone.[9,10] Despite recent advances in the treatment of patients expressing metastatic CRPC, the average survival period remains approximately 3 years.[11] Therefore, the need to develop more effective therapeutic agents is absolutely paramount to improving overall survival.

Experimental animal models have played a critical role in studying human PCa biology, and developing improved diagnostic and therapeutic approaches. In recent years, efforts to develop a preclinical PCa model have yielded numerous breakthroughs.[12] Various mouse models of PCa have proven extremely valuable in expanding our knowledge of PCa. These PCa models have continued to become more robust and have expanded to include a wide variety of transgenic, knockout, and xenograft mouse models.[13] However, mouse models are very small and they are phylogenetically far from human models. To improve detection and treatment options further, an animal model of PCa larger than the existing rodent models has become necessary. Additionally, a model with more physiological, anatomical, and organic similarities to humans will make it easier to predict how the treatment will perform in humans.[14] Larger models exist like the canine model[15] but are limited because they are more expensive to maintain, less available due to a limited number of vendor providers, and it is difficult to obtain older male dogs necessary for these studies. In this regard, rabbits are a good alternative because of their intermediate size between rodent and canine models, availability, and ease of use for experimental procedures.

Rabbits are commonly used in biomedical research as they are more phylogenetically similar to humans than rodents[16] and are more economical and available than dogs. Due to their short life spans, short gestation periods, high numbers of progeny, and low cost compared to other large animals, rabbits often serve to bridge the gap between smaller rodents (mice and rats) and larger animals, such as dogs, pigs, and monkeys.[16] Despite the absence of reported literature on a rabbit orthotopic prostate tumor model, in-depth and extensive histological and morphological characterization of the rabbit reproductive/prostate anatomy has been published.[17–23] Here, we report, for the first time, on the development of a novel orthotopic PCa model in the New Zealand White rabbit. Importantly, the rabbit prostate in older animals approaches a human size, with glands of ~1–2 cm in diameter. This allows for inoculation of tumors in a more physiologically-relevant milieu of normal prostate tissue, than is possible in small rodents. This model can better recapitulate the clinical scenario and could be ideal for the development and optimization of imaging-based diagnostic and therapeutic procedures. Utilizing the rabbit model of human PCa could bring more value and significance to results from PCa models in preclinical studies.

2 | MATERIALS AND METHODS

2.1 | Cell culture

Retrovirally transformed prostate-specific membrane antigen (PSMA) positive human PC3pip cells were originally obtained from Dr. Michel

Sadelain (Laboratory of Gene Transfer and Gene Expression, Gene Transfer and Somatic Cell Engineering Facility, Memorial-Sloan Kettering Cancer Center). Cells were further manipulated to express a green fluorescent protein (GFP) by the laboratory of Susann Brady-Kalnay. The cell line was most recently checked and authenticated by Western blot in 2020. Cells were grown at 37°C and 5% CO_2 under a humidified atmosphere. Cells were maintained in Roswell Park Memorial Institute-1640 medium supplemented (Invitrogen Life Technology) with 10% fetal bovine serum.

2.2 | Tumor inoculation

Animals were handled according to a protocol approved by the Institutional Animal Care and Use Committee at Case Western Reserve University and were in accordance with all applicable protocols and guidelines for animal use. Immunosuppression via cyclosporine (10 mg/kg) injected subcutaneously was first performed one day before the tumor cell injection and then injected daily until the end of the study. Twenty male New Zealand White rabbits from 3 to 18 months old with a mean age of 9 months were used in this study and were obtained from Charles River Laboratories. Anesthesia (isoflurane 1%–2%) was maintained throughout all procedures unless otherwise noted. For tumor cell injection, animals were placed in the supine position. The lower abdomen was shaved and then sterilized with iodine. Animals in Group A ($n = 6$) underwent a laparotomy to allow the injection of 8×10^6 PC3pipGFP cells suspended in 50 µl of phosphate-buffered saline (PBS) directly into the middle of the prostate gland via a 29 1/2-Gauge insulin needle (Smiths Medical ASD, Inc). The 29 1/2-Gauge insulin needle is small and has little space in the head of the syringe, allowing safe injection of all the cell suspension into the prostate gland. For animals in Group B ($n = 14$), PC3pipGFP cells were inoculated via US-guided injection. The needle used here was a 21-Gauge (BD PrecisionGlide™ needles) 50.8 mm in length. Because the abdomen was not opened, the needle used was long enough to penetrate the prostate for image-guided tumor cell injection. For these injections, a 1 ml syringe was used to inject the cell suspension into the prostate gland. The needle was introduced through the abdominal skin and progressed to the prostate obliquely. Once the tip of the needle was shown to be proximal to the prostate, the transducer was then manipulated to verify the central placement of the needle within the prostate. Upon reaching the middle of the prostate, 100–200 µl of 8×10^6 cell suspension was injected into the rabbit. To encourage tumor growth within the prostate parenchyma rather than in the subcapsular area, the syringe was changed and a 20 µl solution of sterile surgical tissue glue (Patterson Veterinary Webglue™) was then injected to seal the puncture point in four rabbits in Group B (Subjects 5–8). This resulted in all of the tumor cells (200 µl) injected being pushed all the way to the prostate. We also tested the effect of injection volume on tumor implantation and growth. Subjects 11–14 in Group B were injected with 8×10^6 cells but suspended in 100 µl suspension and without the use of glue. A smaller volume was used, while keeping the number of cells the same, to lower the probability of cells leaking out of the prostate after injection and consequently, avoiding the use of glue as well. Before injection, both the syringe and needle were filled with cells to ensure that 100 µl of 8×10^6 cells were all injected into the prostate. The success of cell injections was verified by the appearance of hyperechoic foci in the prostatic parenchyma in the US image (Figure 1A–D).

2.3 | Tumor imaging

B-mode and Doppler US images for guided tumor cell injection and tumor monitoring were all performed using a Siemens Acuson S3000 US scanner employing an 18 MHz (18L6) center frequency transducer. For contrast-enhanced US examination, the standard nonlinear contrast pulse sequencing (CPS) mode was used to image the change of tissue contrast density (frequency, 8.0 MHz; MI, 0.13; dynamic range, 55 dB; gain, −5 dB; imaging frame rate, 1 frames/s) using the same transducer. Images were acquired trans-abdominally with either sagittal or transverse orientation. Magnetic resonance imaging (MRI) images were obtained with a 3 T Magnetom Vida human MRI scanner (Siemens Healthineers) using the following parameters: echo time = 85 ms, repetition time = 7000 ms, flip angle = 160°, bandwidth = 203 Hz/pixel, voxel size = $0.4 \times 0.4 \times 2.0$ mm^3, field of view = 120×86.3 mm (sagittal) and 120×97.5 mm (transverse), base resolution = 320, 26 slices. MRI was read by a radiologist to determine the location and size of the tumor. Rabbits were anaesthetized and kept sedated by inhalation of isoflurane (3%) before and during the US. Ketamine (10 mg/kg) was administered via intramuscular injection 5–10 min before MRI and 5 mg/kg ketamine was injected when needed via intravenous injection to keep the rabbits sedated during the MRI procedure as monitored by a veterinarian. Following euthanasia at 5 weeks post tumor injection, bladder and tumor tissues were harvested, ex vivo images of tissues were performed on a Maestro In Vivo Imaging System (PerkinElmer) using a blue filter (excitation 445–490 nm, emission filter 515 nm long pass) to detect GFP expressed by the PCa cells.

2.4 | Pathology

Following ex vivo imaging, bladder and tumor tissues were then fixed in formalin, embedded in paraffin, and stained with hematoxylin and eosin (H&E) using standard protocols. Also, for immunohistochemistry (IHC) studies harvested tissue was processed by the Case Comprehensive Cancer Center pathology core for PSMA (ab19071, Ms monoclonal antibody [mAb] to PSMA; Abcam). IHC staining for PSMA expression was performed using a BioCare Medical IntelliPath FLX automated IHC slide stainer. Tissue sections from paraffin blocks were placed on a glass slide and baked at 60°C for 75 min. The tissue sections were then deparaffinized in xylene for 14 min, rehydrated in ethanol, and rinsed in deionized water. Antigen retrieval was performed by placing the slides in citrate buffer and

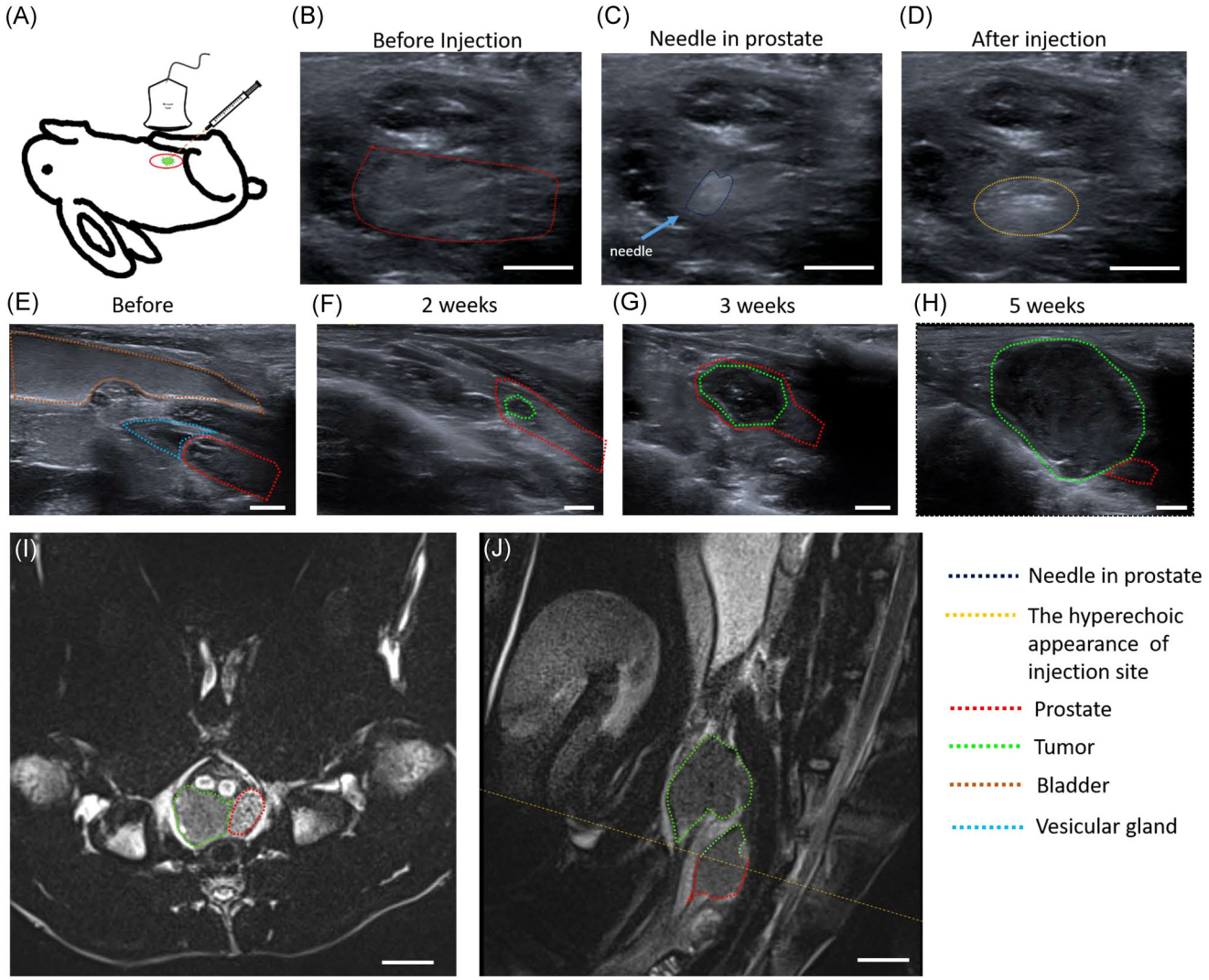

FIGURE 1 Orthotopic injection of PC3pipGFP tumor cells into rabbit prostate under ultrasound guidance: (A) The schematic diagram of tumor model. (B) Normal prostate before injection. (C) Needle in the prostate. (D) Injection of cells was associated with the appearance of hyperechoic foci in the prostatic parenchyma. Sagittal ultrasound image to monitor tumor growth: (E) Image of normal prostate, bladder, and vesicular gland before inoculation. (F) Image of tumor and prostate 2 weeks after inoculation. (G) Image of tumor and prostate 3 weeks after inoculation. (H) Image of tumor and prostate 5 weeks after inoculation. MRI of the tumor: (I) T2 MRI in the transverse plane. (J) T2 MRI in the sagittal plane wherein tumors can be found both inside and outside the prostate. The yellow dotted line corresponds to the MRI in the transverse plane (I). Tumors are outlined in green and prostate in red. Scale bar = 0.5 cm for (B–H) and 1 cm for (I, J). MRI, magnetic resonance imaging [Color figure can be viewed at wileyonlinelibrary.com]

incubated at 125°C for 30 s. The slides were then cooled and rinsed in deionized water. The slides were then treated with Peroxidazed 1 (BioCare Medical) for 8 min, which is a very stable form of hydrogen peroxide used to block endogenous peroxidase activity, and then rinsed with deionized water. The slides were further treated with a blocking agent that is primarily made of purified casein, Background Sniper (BioCare Medical), used to block endogenous immunoglobulin G and charged protein activity, and then rinsed with deionized water. Deparaffinized tissue sections were then incubated in a shaker for 1 h with PSMA antibody (ab19071, Ms mAb to PSMA) that was diluted 1:1000 (vol/vol). A MACH 4 Universal HR-Polymer Kit (BioCare Medical) was then used to detect antibodies using a specific probe and a horseradish peroxidase polymer that binds to the probe. The slides were then incubated for 5 min. in the dark with 3,3′diaminobenzidine (DAB) (Betazoid DAB; BioCare Medical) to reveal the bound antibodies. Tissue sections were then counterstained with ready-to-use hematoxylin (BioCare Medical). The slides were read by a pathologist using a light microscope.

2.5 | Microbubble and nanobubble imaging study

Nanobubble (NB) contrast agents were prepared as previously described and used to image rabbits with PCa cells injected into the

prostate.[24] Briefly, 6 mg DBPC, 1 mg DPPA, 2 mg DPPE, and 1 mg mPEG(2k)-DSPE lipids were weighed and dissolved in 0.1 ml propylene glycol in an 80°C water bath until clear. The lipid solution was then diluted in a mixture of PBS (0.8 ml) and glycerol (0.1 ml). After rabbits were anesthetized with isoflurane, each rabbit was placed in the face-up position, and the US probe (18L6) was placed longitudinally to the axis of the rabbit body to visualize the US images of the tumor. To compare NB images with the same tumor in the same rabbit, different doses of NBs were delivered to animals by adjusting the volume of NBs. Animals obtained a baseline US image without NB injection and then received NB doses as follows: 0.3, 0.5, 0.7, 1.0, and 1.5 ml. After injection of NBs, CPS was used to image the change of tissue contrast density (frequency, 8.0 MHz; MI, 0.13; dynamic range, 55 dB; gain, −5 dB; imaging frame rate, 1 frame/s). Rabbits were imaged continuously for 20 min. After that, US energy was increased to burst the NBs and were allowed to clear from the body for another 20 min before the next NB administration.[2] A similar procedure was performed using clinically approved Lumason microbubbles (MBs) for comparison with the following doses: 0.3, 0.5, 0.7, and 1.5 ml.

3 | RESULTS

3.1 | Inoculation procedure and general imaging characteristics

The purpose of this study is to establish, characterize, and optimize an orthotopic human PSMA-expressing, prostate tumor model in rabbits. In this study, 14 out of 20 rabbits grew tumors. Two methods were used for tumor inoculation. In Group A, tumor cells were injected directly into the prostate gland via an invasive laparotomy ($n = 6$). In Group B, tumor cells were injected in a minimally-invasive manner by using transabdominal percutaneous injection under US guidance ($n = 14$). As is shown in Table 1, PC3pipGFP tumor grew in three rabbits after an invasive laparotomy, and in 11 rabbits after using a transabdominal percutaneous injection under US guidance. Among the six rabbits that did not grow tumors, two factors stood out: rabbit age and tumor inoculation method (Table S1). Three out of four of the 18 months old rabbits did not grow tumors. This may be due to the rabbits not being able to tolerate cyclosporine well and having to be euthanized at 2–3 weeks following tumor cell injection before tumor growth was detected. Overall, laparotomy resulted in a 50% success rate (three out of six) and transabdominal percutaneous injection under US guidance was at a 79% success rate (11 out of 14), wherein three of the rabbits that did not grow tumors were 18 months old. In addition, rabbits that grew tumors had an average age of 8 months while those that did not have an average age of 12 months.

The rabbits in this study have prostates with a mean size of 85 ± 26 mm^2 and were detected via the US. Occasionally, anatomical differences in the location of the prostate gland relative to the pelvic bones made localizing and visualizing the prostate gland and/or the tumor growth more difficult. This issue was more prevalent with the sagittal imaging plane. After tumor inoculation via laparotomy, follow-up imaging exams had to be delayed until 2–3 weeks following the surgical procedure, to allow for proper wound healing. In contrast, for US-guided injection, there was no such limitation and a US scan could be performed 1 week after tumor inoculation.

3.2 | Tumor growth monitoring

Before inoculation of tumor cells into the prostate gland the healthy prostate, bladder, and vesicular glands were imaged with the US, Figure 1E, to achieve a baseline control dataset. Prostate glands of the rabbits had a mean cross-sectional area of 85 ± 26 mm^2 (ranging from 46 to 151 mm^2) and increased in size with rabbit age. Following cell injection, tumor progression was observed over time with continued weekly US scans as shown in Figure 1F–H.

3.3 | Tumor location verification

MRI was utilized to verify the location of the prostate gland and tumor and to examine features of the lesions using another imaging modality. The tumor presence was verified with MRI 3–5 weeks following inoculation as shown in Figure 1I,J. Tumors are shown in sagittal and transverse planes, which were read by a radiologist. The tumor growth rate was 39 ± 25 mm^2 per week. Figure 2 shows a steady increase in tumor size relative to the number of weeks after the rabbit was inoculated with tumor cells.

The presence of PC3pipGFP PCa tumor cells and their distribution within the prostate and nearby organs, such as the bladder, was also verified through fluorescence imaging 5 weeks post-inoculation for a subset of animals. The rabbits were euthanized, tumors were removed, and imaged ex vivo. As shown in Figure 3, fluorescence imaging identified GFP signals coming from tumors previously identified on MRI. These data confirmed the growth and location of the PC3pipGFP tumor in the immunosuppressed animal. As shown in Figure 1F,G, small tumors that are less than 1 cm^2 were found in the parenchyma of the prostate. Larger tumors (Figure 1H), bigger than 4 cm^2, partially protruded from the prostate gland. From Table 1, 7 out of 14 cases observed in this study found tumors both inside and outside the prostate, which is also shown in a representative 5-week explanted rabbit prostate tumor (Figure 3). In this case, one of the tumors was totally outside the prostate while the other tumor was partly in and outside of the prostate showing that the tumor grew outside of the boundaries of the prostate gland. The location of tumors outside of the gland and not contiguous to the tumor within the gland may have grown from tumor cells upon withdrawal of the needle from the gland following injection. There was no correlation between the use of glue and the growth of the tumor exclusively within the gland, suggesting that surgical glue is not an efficient means to keep tumor cells from emerging from the gland.

TABLE 1 Summary of 14 subjects that grew tumors

Group	Subject	Age during tumor inoculation	Tumor Inoculation	Gland identification before tumor cell injection	PC3pip GFP cells injected (volume/number)	Time of sacrifice rabbits after tumor cell injection	Successful tumor growth via necropsy	Tumor size (cm; $l \times w$) in 5 weeks via US after cell injection/at endpoint week	Tumor location (inside or outside prostate) via necropsy
A	1	3 months	Surgery	Yes	50 µl/8 × 10^6	9 weeks	Yes	N/A[a]	Inside/outside
A	2	6 months	Surgery	Yes	50 µl/8 × 10^6	8 weeks	Yes	1.1 × 0.6	Inside/outside
A	3	6 months	Surgery	Yes	50 µl/8 × 10^6	8 weeks	Yes	1.3 × 0.9	Inside/outside
B	4	6 months	Injection	Yes	150 µl/6 × 10^6	8 weeks	Yes	1.0 × 0.9	Inside/outside
B	5	18 months	Injection	Yes	200 µl/8 × 10^6	5 weeks	Yes	2.5 × 2.0	Inside/outside
B	6	6 months	Injection	Yes	200 µl/8 × 10^6	6 weeks	Yes	1.39 × 1.26	Outside
B	7	6 months	Injection	Yes	200 µl/8 × 10^6	6 weeks	Yes	1.09 × 0.83	Outside
B	8	6 months	Injection	Yes	200 µl/8 × 10^6	6 weeks	Yes	1.42 × 1.10	Inside
B	9	6 months	Injection	Yes	200 µl/8 × 10^6	6 weeks	Yes	1.08 × 1.25	Outside
B	10	5 months	Injection	Yes	200 µl/8 × 10^6	5 weeks	Yes	1.47 × 1.40	Outside
B	11	9 months	Injection	Yes	100 µl/8 × 10^6	4 weeks	Yes	1.98 × 1.37	Inside
B	12	9 months	Injection	Yes	100 µl/8 × 10^6	7 weeks	Yes	1.97 × 1.63	Inside
B	13	12 months	Injection	Yes	100 µl/8 × 10^6	5 weeks	Yes	1.65 × 1.49 1.20 × 1.12 1.51 × 0.63	Inside/outside
B	14	12 months	Injection	Yes	100 µl/8 × 10^6	4 weeks	Yes	1.90 × 1.83 0.89 × 0.82	Inside/outside

Abbreviations: GFP, green fluorescent protein; US, ultrasound.

[a]The tumor was deep in the pelvis and the bone blocked the signal, not detectable by US.

3.4 | Histology analysis

Following tissue harvesting, H&E and IHC staining were also used to confirm the presence and location of cancerous tissue in the rabbit prostate gland. H&E staining reveals the presence of both the normal prostate gland and PCa (Figure 4A–F). Staining using anti-PSMA antibodies, Figure 4G–J showed the expression of PSMA within the explanted tissues. Low levels of PSMA expression were detected in normal prostate tissues. In contrast, PCa expressed exceedingly high levels of PSMA expression. It is notable that the main tumor mass identified by H&E staining was also positive for PSMA suggesting the utility of PSMA as a biomarker for PCa in the rabbit model.

3.5 | US contrast agent detection of NBs

Image-guided PCa detection using US and, at times, contrast-enhanced US is an important part of the PCa diagnosis workflow.[2,24] As such, we carried out experiments to examine the tumor enhancement kinetics using experimental NB contrast agent and standard clinical US contrast agent (Lumason) as well. NBs and Lumason MBs were injected intravenously via an ear vein and the tumor enhancement was evaluated at different doses (Figure 5 and Figure S1, respectively).

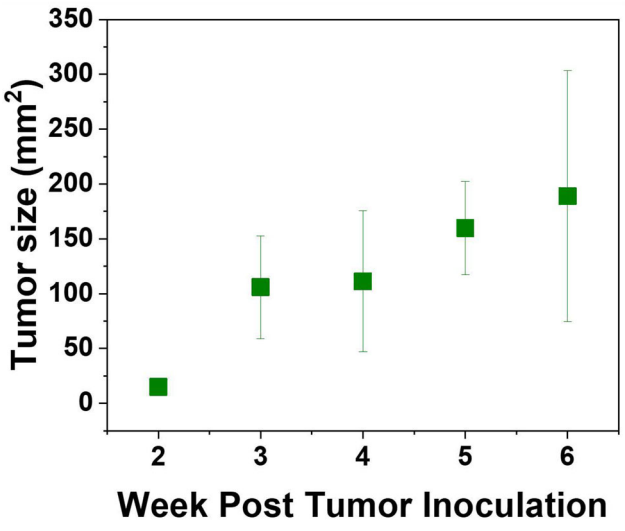

FIGURE 2 Plot of tumor size relative to the number of weeks post tumor inoculation [Color figure can be viewed at wileyonlinelibrary.com]

The vascularity of orthotopically implanted human PCa in this rabbit model can be detected using both color Doppler flow imaging and pulse wave Doppler, wherein the blood flow of relatively big vessels can be observed (Figure 5B). In contrast to Doppler imaging, administration of NB-US contrast agents into the rabbits can detect microcirculation and small vessels in the tumor that can be seen filling with NBs (Figure 5C). However, MBs administration did not enhance tumor contrast except at the periphery of the tumor (Figure S1).

A goal in developing this model was the development of a reasonably sized tumor to better understand contrast agent dosing and kinetics in vivo in tumors compared to normal prostate tissue. To examine the optimal NB dose required for tumor detection, different doses of NBs were injected IV, and the effect of dose on the distribution of NBs in the tumor and iliac artery ($n = 3$) was determined. Doses were randomly administered to the tumor-bearing rabbits to minimize bias. After imaging and data collection, high-energy US was administered to completely destroy residual NBs and were allowed to clear from the animal body for 20 min before the next injection.[25] It was found that as injection volume increased, the peak intensity increased and the signal in the tumor area became brighter as shown in Figure 5C–E. In contrast, the signal in the artery remained constant for all doses. The peak intensities of 0.3, 0.5, 0.7, 1.0, and 1.5 ml NBs were 9.1 ± 1.1, 25.5 ± 8.4, 34.1 ± 11.4, 50.5 ± 13.4, and 66.6 ± 14.9, respectively, in tumors, and 150 ± 45.3, 156.8 ± 43.8, 163.1 ± 45.3, 163.5 ± 44.8, and 166.1 ± 43.4, respectively, in iliac arteries. Peak signal intensities in the iliac artery were comparable between different NB doses. In contrast, signal intensity was dependent on administered NB dose, wherein contrast images became brighter with increasing NB dose injected.

Contrast-enhanced ultrasound (CEUS) was also performed on rabbit tumors using clinical Lumason MBs, which showed lower signal enhancement in tumors (Figure S1) compared to NBs (Figure 5C) at the CPS pulse sequence used. This observation may be due to its larger size and lower stability to US exposure compared to NBs, which was previously reported by our group in mouse models.[24] Another reason could be that the CEUS settings used in this study are not tailored to the resonant frequency of the Lumason MBs, which are not the same as that of the NBs because of differences in size and material shell composition.[26,27]

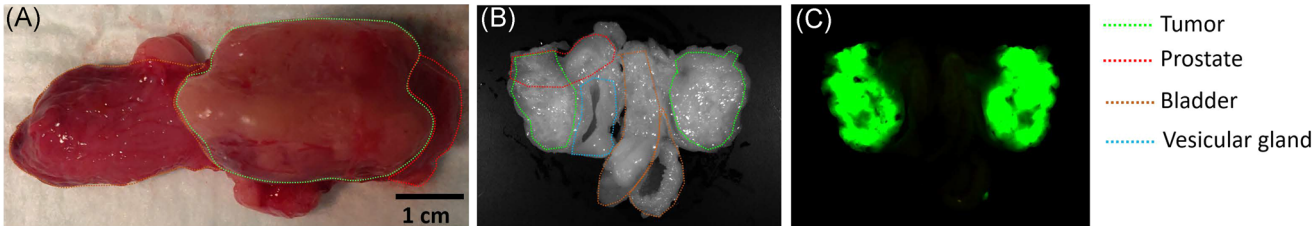

FIGURE 3 Representative gross and fluorescence imaging of the tumor: (A) Gross image of harvested organs. (B) The white light image of harvested organs. (C) Fluorescence image of green fluorescent protein-labeled tumor cells. Here the tissue was cut in half, the images show both sides of the cut organs and tumor [Color figure can be viewed at wileyonlinelibrary.com]

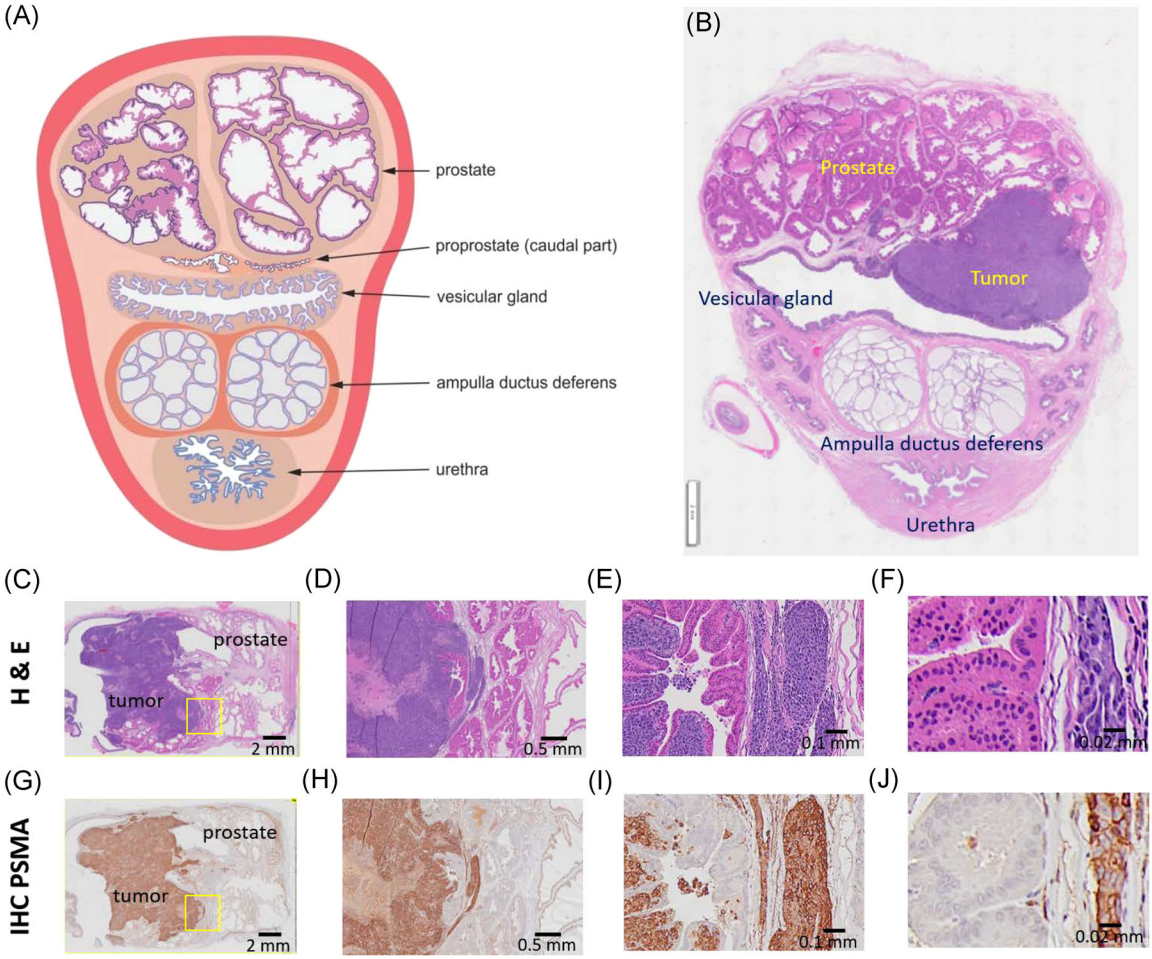

FIGURE 4 (A) Schematic cross-section of the prostate gland complex of the rabbit. (B) Representative histology H&E staining of the rabbit prostate gland region with a tumor in the prostate. These figures appear in an upside-down configuration in US and MRI as the urethra is the most anterior part in the supine position. (A) Reprinted with permission from Skonieczna et al.[18] Representative histology of PC3pipGFP prostate tumor tissue and normal prostate in the rabbit with (C–F) H&E and (G–J) IHC staining. (C–F) Show poorly differentiated malignant tumor cells, staining dark purple, infiltrate the stroma of prostatic glandular tissue. The normal prostatic cells show abundant cytoplasm with light pink staining. (G–J) The malignant cells show diffuse strongly positive immunostaining for PSMA. The nonmalignant native rabbit cells show no immunoreactivity to this antibody. (D, H) Correspond to ×2 image magnification, (E, I) to ×20 image magnification, and (F, J) to ×40 magnification. The yellow squares correspond to the higher magnified areas. H&E, hematoxylin and eosin; IHC, immunohistochemistry; MRI, magnetic resonance imaging; PSMA, prostate-specific membrane antigen; US, ultrasound [Color figure can be viewed at wileyonlinelibrary.com]

4 | DISCUSSION

Several in vitro preclinical models have been established to mimic prostate tumorigenesis and clarify the pathophysiology of PCa. These systems allow for the advancement of the field to first detect prostate cancer and then deliver a novel therapeutic strategy.[28] Cell line-based systems can be a useful way to understand the biology of PCa and test potential therapeutic applications. Several human PCa cell lines from clinical metastatic lesions have been utilized for decades, such as DU-145, PC-3, and LNCaP cells.[29,30] However, these systems are not robust enough for understanding complete tumor biology. Since these cells are two-dimensional monolayers, they do not accurately mimic a clinical situation. To overcome the limitations of cancer cell lines, a wide variety of animal models in immunocompromised rodents, especially mice, have been developed for PCa detection and treatment.[12,31] As a result of their poor ability to translate to the clinical setting, they have been replaced by xenograft and genetically engineered mouse models.[13] Despite the advantages of these systems, mice and rats are not always suitable for studies due to their small sizes and phylogenetic features.[32] Alternatively, rabbit models have considerable advantages over mouse models[33] due to their intermediate size and phylogenetic proximity to primates. These characteristics allow for rabbits to more accurately model the outcomes of diagnostic and therapeutic procedures that will eventually be performed in human clinical practice, including image-guided detection and interventions.[34,35] Canine models of PCa have also been reported[15] and are closer to physiological size compared to human prostate glands. However, they are limited due to higher costs and lower availability of

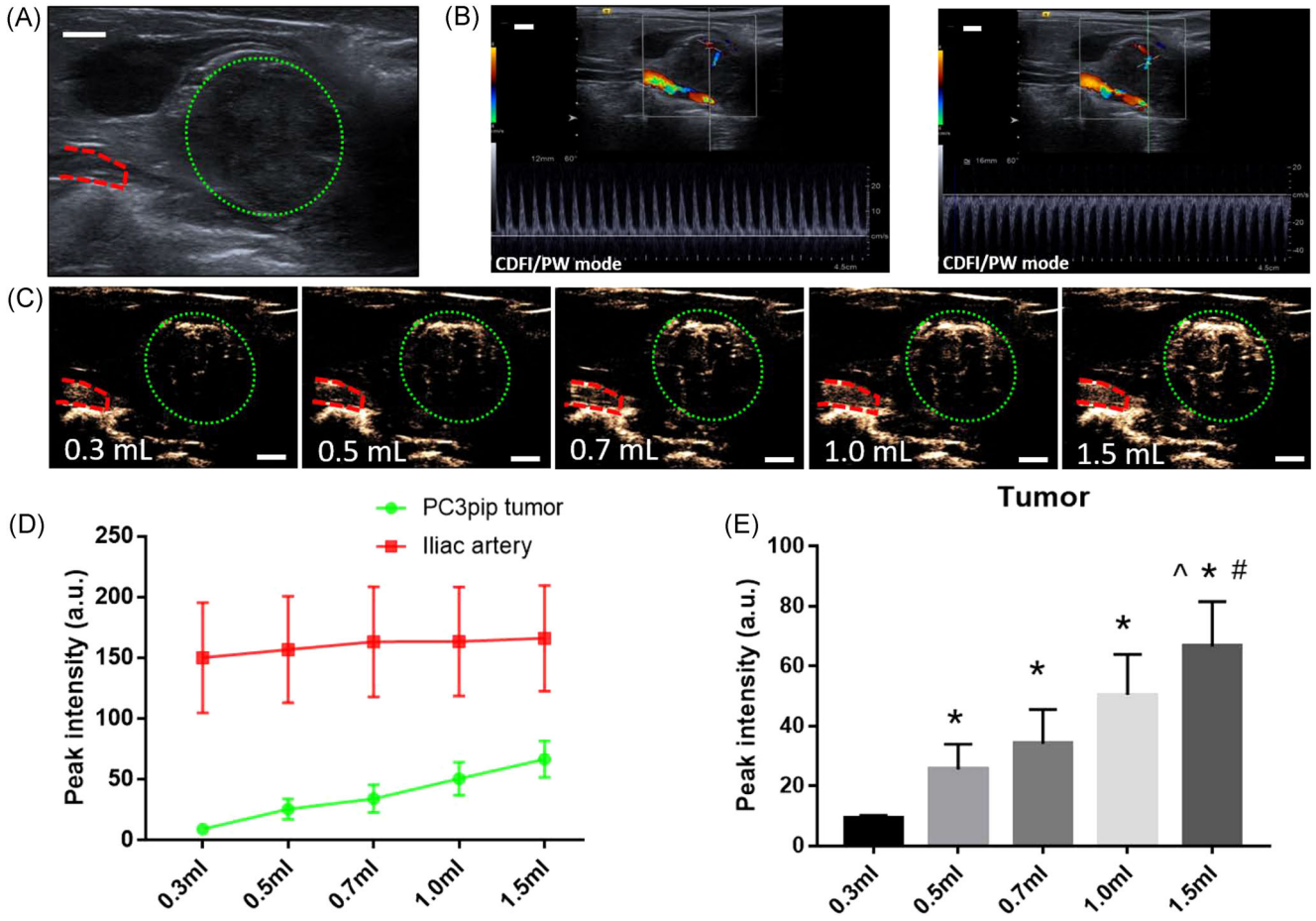

FIGURE 5 (A) Image of tumor in B mode US imaging. (B) Images of tumor in CDFI and PW mode. (C) Images of tumor peak intensity in contrast mode with varying doses of NBs injection. Green dotted circles denote tumor area and red dashed lines indicate the iliac artery. (D, E) Peak intensity of different doses of NBs injection in tumor and artery. Scale bar = 0.5 cm. $^{\wedge}p < 0.05$ with Group 0.5 ml, $^{\#}p < 0.05$ with Group 0.7 ml $^{*}p < 0.05$ with Group 0.3 ml. CDFI, color Doppler flow imaging; NB, nanobubble; PW, pulse wave; US, ultrasound [Color figure can be viewed at wileyonlinelibrary.com]

older male dogs. Thus, rabbits can serve as a bridge between rodents and canine models for PCa studies, supplying important data to support translation to the more expensive canine model.

To date, the most commonly used rabbit tumor model is the rabbit VX2 tumor model, which was developed in 1930–1940 by Rous et al.[36,37] This model has played a longstanding role in experimental and interventional oncology. Since its introduction, the model has been applied for the treatment of several cancer models, such as brain,[38] head and neck,[39] lung,[40] liver,[41,42] pancreas,[43] kidney,[44] urinary bladder,[45] uterus,[46] and bone,[47] but there is no report describing a rabbit orthotopic prostate tumor model.[48] Herein, we have reported, for the first time, the establishment of a novel human castration-resistant, PSMA-expressing orthotopic PCa in a rabbit prostate gland. This model can provide a new platform for performing imaging studies, optimizing diagnostic imaging techniques, evaluating contrast agent kinetics, and examining the efficacy of image-guided interventions such as tumor ablations and external beam radiation.[49]

Through testing of various model parameters, such as rabbit age, injection volume of tumor cells, injection route, and imaging orientation, we have developed a series of "best practices" for the successful instillation of this model in future studies. Here, we summarize our observations and recommendations. First, the age of the rabbit is critical to the successful instillation of the tumors. In younger rabbits, the prostate size was small ($48 \pm 2\ mm^2$) and we observed that rabbits aged 6–12 months with a larger prostate ($83 \pm 15\ mm^2$) were easier to detect the prostate during imaging. This translates to easier tumor cell injection and more precise monitoring of tumor growth, both of which are crucial in in vivo animal cancer studies for both diagnostic and therapeutic applications. Second, we found that 18-month-old rabbits, despite having a larger prostate ($117 \pm 30\ mm^2$), do not tolerate cyclosporine well and three out of four rabbits in this study had to be euthanized due to complications following cyclosporine injection. Rabbit tumors were visible via US imaging as early as 2 weeks after tumor cell injection. The tumor and prostate tissue were easy to distinguish in US imaging and, thus, can be used as an in vivo cancer model for the development of novel diagnostic (e.g., contrast imaging agent efficiency and stability) and therapeutic (drug delivery and efficacy) materials. In this study, three study personnel performed

US-guided tumor cell injections in different rabbits, and tumors grew in all cases. In addition, successful orthotopic tumor growth was observed for the two study personnel who performed injections in multiple rabbits. This indicates that the US-guided technique is easy to learn, reproducible, and operator-independent. At present, this model would enable immediate applications in preclinical studies of CRPC. However, other clinical scenarios (i.e., PCa detection, localization, and staging) would be subject to further investigations based on the underlying differences in comparative anatomy between humans and rabbits. In addition, other cell types and tumor lineages would need to be tested in future iterations, to even more closely emulate the clinical behavior of mid/high risk localized PCa.

CEUS imaging exams were performed to demonstrate that this tumor model can be visualized using this technique. The tumor appears to be relatively highly vascularized compared to the normal prostate, which is consistent with human PCa imaging features.[50,51] Data suggests that for vascular imaging 0.09 ml NBs (equivalent to 1×10^{10} NBs) per kg of rabbit is a sufficient dose. In contrast, proper tumor enhancement, is strongly dose-dependent. An increase in the volume of the NBs, that is, an increase in the number of NBs, resulted in an enhancement of the contrast signal peak intensity with an injection of 1.5 ml of NBs resulting in the highest peak signal intensity in the tumor (Figure 5E). This could be due to higher microvascular vascular density in the tumors where an increase in bubble volume injected results in a higher bubble concentration per imaging voxel, thus giving stronger backscatter. It could also be a result of NB extravasation, which could reduce the circulating bubble concentration until a critical amount of bubbles is reached.

5 | CONCLUSION

This study has successfully demonstrated, for the first time, that human origin, PSMA-expressing orthotopic prostate tumors can be successfully initiated in the New Zealand White rabbits. The model shows robust progression, has imaging features similar to human tumors and exhibits a morphology that is close to human PCa. The tumor also expresses the PSMA receptor, and, thus, can be utilized for optimizing and developing new targeted imaging and therapeutic approaches to this biomarker. Large animals are critical for demonstrating the capabilities of many technologies, including scale-up of nanoparticle-based approaches, and image-guided interventions. As such, the orthotopic PCa rabbit model developed here holds the potential to advance similar studies in other areas such as imaging, chemotherapy, surgical therapy, and local ablative therapy.

ACKNOWLEDGMENTS

This study was supported by the Case-Coulter Translational Research Partnership and Wallace H. Coulter Foundation (Agata A. Exner and James P. Basilion). This study was also supported by the National Institutes of Health via the National Institute of Biomedical Imaging and Bioengineering under Award No. R01EB025741. The authors would like to thank Dr. Michael Tweedle of Ohio State University for helpful discussions in developing this study; Dr. Leonardo K. Bittencourt for his expertise and knowledge in magnetic resonance imaging (MRI); Dr. Kristie Brock, Lynnette Carlton, Shelly Weisman, Marissa O'Callaghan, and Melissa Dusek of the CWRU Animal Resource Center for assistance with the rabbit experiments; and Susan Farr and Michael Markley of the Case Center for Imaging Research for their help with MRI. They would also like to thank Siemens Healthcare for their support of the clinical US system.

CONFLICT OF INTERESTS

The authors declare no conflict of interest.

DATA AVAILABILITY STATEMENT

The data that support the findings of this study are available from the corresponding author upon reasonable request.

ORCID

Eric C. Abenojar http://orcid.org/0000-0002-2733-4006
Xinning Wang https://orcid.org/0000-0001-7729-0534
James P. Basilion https://orcid.org/0000-0002-8659-3307
Agata A. Exner https://orcid.org/0000-0003-3913-7066

REFERENCES

1. Prostate Cancer—Cancer Stat Facts. Accessed April 25, 2021. https://seer.cancer.gov/statfacts/html/prost.html
2. Perera RH, de Leon A, Wang X, et al. Real time ultrasound molecular imaging of prostate cancer with PSMA-targeted nanobubbles. *Nanomed: Nanotechnol, Biol Med*. 2020;28:102213.
3. Mottet N, Bellmunt J, Bolla M, et al. EAU-ESTRO-SIOG guidelines on prostate cancer. Part 1: screening, diagnosis, and local treatment with curative intent. *Eur Urol*. 2017;71:618-629.
4. Roethke M, Anastasiadis AG, Lichy M, et al. MRI-guided prostate biopsy detects clinically significant cancer: analysis of a cohort of 100 patients after previous negative TRUS biopsy. *World J Urol*. 2012;30:213-218.
5. Pallwein L, Mitterberger M, Pelzer A, et al. Ultrasound of prostate cancer: recent advances. *Eur Radiol*. 2008;18:707-715.
6. Siegel RL, Miller KD, Jemal A. Cancer statistics, 2019. *CA Cancer J Clin*. 2019;69:7-34.
7. Dehm SM, Schmidt LJ, Heemers HV, Vessella RL, Tindall DJ. Splicing of a novel androgen receptor exon generates a constitutively active androgen receptor that mediates prostate cancer therapy resistance. *Cancer Res*. 2008;68:5469-5477.
8. Chen X, Li Q, Liu X, et al. Defining a population of stem-like human prostate cancer cells that can generate and propagate castration-resistant prostate cancer. *Clin Cancer Res*. 2016;22:4505-4516.
9. Cookson MS, Roth BJ, Dahm P, et al. Castration-resistant prostate cancer: AUA guideline. *J Urol*. 2013;190:429-438.
10. Heidenreich A, Bastian PJ, Bellmunt J, et al. EAU guidelines on prostate cancer. Part II: treatment of advanced, relapsing, and castration-resistant prostate cancer. *Eur Urol*. 2014;65:467-479.
11. Roviello G, Sigala S, Sandhu S, et al. Role of the novel generation of androgen receptor pathway targeted agents in the management of castration-resistant prostate cancer: a literature based meta-analysis of randomized trials. *Eur J Cancer*. 2016;61:111-121.
12. Russell PJ, Voeks DJ. Animal models of prostate cancer. Russell PJ, Jackson P, Kingsley EA, eds, *Prostate Cancer Methods and Protocols*. Methods in Molecular Medicine. Vol 81. 1st ed. Springer, 2003:89-112.
13. Wang F. Modeling human prostate cancer in genetically engineered mice. *Progress in Molecular Biology and Translational Science*. Vol 100. Elsevier B.V; 2011:1-49.

14. Harcourtbrown F. Biological characteristics of the domestic rabbit (*Oryctolagus cuniculi*). *Textbook of Rabbit Medicine*. Elsevier; 2002: 1-18.
15. Keller JM, Schade GR, Ives K, et al. A novel canine model for prostate cancer. *Prostate*. 2013;73:952-959.
16. Fan J, Chen Y, Yan H, Niimi M, Wang Y, Liang J. Principles and applications of rabbit models for atherosclerosis research. *J Atheroscler Thromb*. 2018;25:213-220.
17. Foote RH, Carney EW. The rabbit as a model for reproductive and developmental toxicity studies. *Reprod Toxicol*. 2000;14:477-493.
18. Skonieczna J, Madej JP, Będziński R. Accessory genital glands in the New Zealand White rabbit: a morphometrical and histological study. *J Vet Res*. 2019;63:251-257.
19. Holtz W, Foote RH. The anatomy of the reproductive system in male Dutch rabbits (*Oryctolagus cuniculus*) with special emphasis on the accessory sex glands. *J Morphol*. 1978;158:1-20.
20. Sohn J, Couto MA. Anatomy, physiology, and behavior. *The Laboratory Rabbit, Guinea Pig, Hamster, and Other Rodents*. Elsevier Inc.; 2012:195-215.
21. Skonieczna J, Madej JP, Kaczmarek- Pawelska A, Będziński R. Histological and morphometric evaluation of the urethra and penis in male New Zealand White rabbits. *J Vet Med Ser C, Anat Histol Embryol*. 2021;50:136-143.
22. Onuoha CH. Reproductive physiology of male rabbits: a key factor in buck selection for breeding (paper review). *Adv Reprod Sci*. 2020;8: 97-112.
23. Ittmann M. Anatomy and histology of the human and murine prostate. *Cold Spring Harb Perspect Med*. 2018;8:a030346.
24. De Leon A, Perera R, Hernandez C, et al. Contrast enhanced ultrasound imaging by nature-inspired ultrastable echogenic nanobubbles. *Nanoscale*. 2019;11:15647-15658.
25. Johansen ML, Perera R, Abenojar E, et al. Ultrasound-based molecular imaging of tumors with PTPmu biomarker-targeted nanobubble contrast agents. *Int J Mol Sci*. 2021;22:1983.
26. Talu E, Hettiarachchi K, Zhao S, et al. Tailoring the size distribution of ultrasound contrast agents: possible method for improving sensitivity in molecular imaging. *Mol Imaging*. 2007;6:384-392.
27. Dicker S, Mleczko M, Siepmann M, et al. Influence of shell composition on the resonance frequency of microbubble contrast agents. *Ultrasound Med Biol*. 2013;39:1292-1302.
28. Namekawa T, Ikeda K, Horie-Inoue K, Inoue S. Application of prostate cancer models for preclinical study: advantages and limitations of cell lines, patient-derived xenografts, and three-dimensional culture of patient-derived cells. *Cells*. 2019;8:74.
29. Sobel RE, Sadar MD. Cell lines used in prostate cancer research: a compendium of old and new lines—part 1. *J Urol*. 2005;173:342-359.
30. Sobel RE, Sadar MD. Cell lines used in prostate cancer research: a compendium of old and new lines—part 2. *J Urol*. 2005;173: 360-372.
31. Pienta KJ, Abate-Shen C, Agus DB, et al. The current state of preclinical prostate cancer animal models. *Prostate*. 2008;68:629-639.
32. Peng X. Transgenic rabbit models for studying human cardiovascular diseases. *Comp Med*. 2012;62:472-479.
33. Mapara M, Thomas B, Bhat K. Rabbit as an animal model for experimental research. *Dent Res J*. 2012;9:111-118.
34. Bertolini F, Schiavo G, Scotti E, et al. High-throughput SNP discovery in the rabbit (*Oryctolagus cuniculus*) genome by next-generation semiconductor-based sequencing. *Anim Genet*. 2014;45:304-307.
35. Yang D, Xu J, Zhu T, et al. Effective gene targeting in rabbits using RNA-guided Cas9 nucleases. *J Mol Cell Biol*. 2014;6:97-99.
36. Rous P, Beard JW. The progression to carcinoma of virus-induced rabbit papillomas (shope). *J Exp Med*. 1935;62:523-548.
37. Kidd JG, Rous P. A transplantable rabbit carcinoma originating in a virus-induced papilloma and containing the virus in masked or altered form. *J Exp Med*. 1940;71:813-838.
38. Frank JA, Girton M, Dwyer AJ, et al. A reproducible model of metastatic brain and ocular tumor by hematogenous inoculation of the VX2 tumor in rabbits. *J Neurosurg*. 1987;67:106-109.
39. Van Es,RJJ, Dullens HFJ, Van Der Bilt A, Koole R, Slootweg PJ. Evaluation of the VX2 rabbit auricle carcinoma as a model for head and neck cancer in humans. *J Cranio-Maxillofac Surg*. 2000;28: 300-307.
40. Anayama T, Nakajima T, Dunne M, et al. A novel minimally invasive technique to create a rabbit VX2 lung tumor model for nano-sized image contrast and interventional studies. *PLoS One*. 2013;8:e67355.
41. Park JS, Withers SS, Modiano JF, et al. Canine cancer immunotherapy studies: linking mouse and human. *J Immunother Cancer*. 2016;4:1-11.
42. Hoye RC, Thomas LB, Riggle GC, Ketcham A. Effects of neodymium laser on normal liver and VX2 carcinoma transplanted into the liver of experimental animals. *J Natl Cancer Inst*. 1968;41:1071-1082.
43. Eifler AC, Lewandowski RJ, Virmani S, et al. Development of a VX2 pancreatic cancer model in rabbits: a pilot study. *J Vasc Interv Radiol*. 2009;20:1075-1082.
44. Lee JM, Kim SW, Chung GH, Lee SY, Han YM, Kim CS. Open radiofrequency thermal ablation of renal VX2 tumors in a rabbit model using a cooled-tip electrode: feasibility, safety, and effectiveness. *Eur Radiol*. 2003;13:1324-1332.
45. Yang WH, Liebert M, Price RE, Cromeens DM, Lin JS, Grossman BH. Extravesical cryosurgical approach for VX2 bladder tumor in rabbits. *Urol Res*. 2001;29:345-349.
46. Rhee TK, Ryu RK, Bangash AK, et al. Rabbit VX2 tumors as an animal model of uterine fibroids and for uterine artery embolization. *J Vasc Interv Radiol*. 2007;18:411-418.
47. Handal JA, Schulz JF, Florez GB, Kwok SCM, Khurana JS, Samuel SP. Creation of rabbit bone and soft tissue tumor using cultured VX2 cells. *J Surg Res*. 2013;179:e127-e132.
48. Galasko CSB, Muckle DS. Intrasarcolemmal proliferation of the VX2 carcinoma. *Br J Cancer*. 1974;29:59-65.
49. Eichelberger LE, Koch MO, Eble JN, Ulbright TM, Juliar BE, Cheng L. Maximum tumor diameter is an independent predictor of prostate-specific antigen recurrence in prostate cancer. *Mod Pathol*. 2005;18: 886-890.
50. Panagiotaki E, Chan RW, Dikaios N, et al. Microstructural characterization of normal and malignant human prostate tissue with vascular, extracellular, and restricted diffusion for cytometry in tumours magnetic resonance imaging. *Invest Radiol*. 2015;50:218-227.
51. Lovegrove CE, Matanhelia M, Randeva J, et al. Prostate imaging features that indicate benign or malignant pathology on biopsy. *Transl Androl Urol*. 2018;7:S420-S435.

SUPPORTING INFORMATION

Additional supporting information may be found in the online version of the article at the publisher's website.

How to cite this article: Wang Y, Abenojar EC, Wang J, et al. Development of a novel castration-resistant orthotopic prostate cancer model in New Zealand White rabbit. *The Prostate*. 2022;82:695-705. doi:10.1002/pros.24314